



Carbon for Energy Storage Derived from Granulated White Sugar by Hydrothermal Carbonization and Subsequent Zinc Chloride Activation

M. Härmas, T. Thomberg, T. Romann, A. Jänes,^{*,z} and E. Lust*

Institute of Chemistry, University of Tartu, 50411 Tartu, Estonia

Various electrochemical methods have been applied to establish the electrochemical characteristics of the electrical double layer capacitor consisting of the activated carbon material based electrodes and 1 M triethylmethylammonium tetrafluoroborate solution in acetonitrile and 1-ethyl-3-methylimidazolium tetrafluoroborate ionic liquid as the electrolytes. Activated carbon material used for the preparation of electrodes has been synthesized from hydrochar prepared via hydrothermal carbonization process of granulated white sugar solution in H₂O, followed by activation with ZnCl₂ with a mass ratio of 1:4 at the temperature 700°C. High porosity and Brunauer-Emmett-Teller specific surface area ($S_{\text{BET}} = 2100 \text{ m}^2 \text{ g}^{-1}$), micropore surface area ($S_{\text{micro}} = 2080 \text{ m}^2 \text{ g}^{-1}$) and total pore volume ($V_{\text{tot}} = 1.05 \text{ cm}^3 \text{ g}^{-1}$) have been achieved for the granulated white sugar derived carbon (GWS carbon) material. Wide region of ideal polarizability ($\Delta E \leq 3.0 \text{ V}$), short characteristic relaxation time (0.5 s and 4.0 s), high specific series capacitance (125 F g⁻¹ and 140 F g⁻¹) and high energy density (39 W h kg⁻¹ and 48 W h kg⁻¹) have been calculated for the GWS carbon material in 1 M triethylmethylammonium tetrafluoroborate solution in acetonitrile and 1-ethyl-3-methylimidazolium tetrafluoroborate ionic liquid, respectively, demonstrating that these systems are very promising for energy storage devices.

© The Author(s) 2017. Published by ECS. This is an open access article distributed under the terms of the Creative Commons Attribution 4.0 License (CC BY, <http://creativecommons.org/licenses/by/4.0/>), which permits unrestricted reuse of the work in any medium, provided the original work is properly cited. [DOI: 10.1149/2.0681709jes] All rights reserved.



Manuscript submitted May 11, 2017; revised manuscript received June 21, 2017. Published July 5, 2017.

In recent years, environmentally friendly energy storage devices have gained increasing attention due to the growing requirement of energy storage for sustainable energy applications. Among the various existing energy storage devices, supercapacitors (electrical double layer capacitors (EDLC) and hybrid capacitors (HC)) are considered as the most promising short-term energy storage devices due to their high power density, short characteristic time constant, excellent coulombic reversibility (98% or higher), high energetic efficiency (92–94%), long cycle life (over 10⁶ cycles) and wide operation temperature range^{1–3} filling the gap between dielectric capacitors and traditional batteries.^{4–7} EDLCs store energy in the electrical double layer, where the adsorption of ions is based mainly on the electrostatic interactions. The unique characteristics of EDLCs allow them to replace or combine with batteries and fuel cells in applications where the high power pulses are important, such as the different energy recuperation systems and peak power sources, hybrid electric vehicles, wind turbines, digital communication devices, cameras, mobile phones, laptops, etc.^{8–10}

Porous carbon materials are considered to be the most promising electrode materials for portable supercapacitors due to the high surface area, good electrical conductivity, good chemical stability, low gravimetric density and low cost.^{1–3} The electrical charge accumulated in EDLC depends on the electrochemically active surface area and, thus, on the porosity and hierarchical porous structure of a carbon material. In addition, the presence of mesopores in porous carbon materials determines the power density of EDLC due to a strong effect on the rate of mass transfer (diffusion and migration) and adsorption rate of charge carriers inside the hierarchical porous matrix. Therefore, the characteristics of micro- and mesoporous carbon materials (especially the ratio of micropore and mesopore surface areas and pore volumes) have to be optimized to improve further the specific energy and power density of EDLCs.^{1,11–14}

The classical porous carbon synthesis route uses pyrolysis of organic compounds followed by activation. However, control over pore size distribution by this route is poor. Thus, development of novel methods for the synthesis of porous carbons with controlled pore size distribution is important for further development of supercapacitors technology. Hydrothermal carbonization (HTC) is an attractive process to prepare spherical carbon materials from natural precursors being cheap and “green” since it does not use expensive organic

solvents or catalysts and requires only application of the low processing temperature (normally not higher than 300°C).^{15–20} The process consists of the heat-treatment of an aqueous solution of organic materials at desired autogenous pressure and temperature. The resulting solid carbon product (termed hydrochar) generally possesses very low porosity and additional pyrolysis leads to the moderate increase in porosity of porous carbon materials. Therefore, the carbon material porosity (the pore size distribution, the average pore width and the specific surface area) must be increased by using additional activation methods based on the application of air, carbon dioxide, steam as well as KOH, NaOH, H₃PO₄, etc. as an activation agents.^{21,22}

The objective of this study was to investigate the applicability limits of carbon material derived from granulated white sugar (GWS carbon) by HTC method combined with subsequent zinc chloride activation step of hydrochar, for supercapacitor electrodes. Synthesized GWS carbon material was used as an electrode material in the two-electrode single cells of EDLC filled with 1 M triethylmethylammonium tetrafluoroborate (TEMABF₄) solution in acetonitrile (AN) or 1-ethyl-3-methylimidazolium tetrafluoroborate ionic liquid (EMImBF₄) as the electrolytes. The mixture of TEMABF₄ and AN was selected due to the low viscosity (0.41 mPa s), high electrical conductivity ($\kappa = 50.2 \text{ mS cm}^{-1}$) and good electrochemical stability within a very wide region of cell potentials.^{20,23–27} EMImBF₄ was chosen due to high bulk conductivity ($\kappa = 13.6 \text{ mS cm}^{-1}$) and wide potential region of electrochemical stability.^{28–31} However, compared to TEMABF₄ solution in AN, EMImBF₄ has almost two order of magnitude higher viscosity (38.2 mPa s).³² Cyclic voltammetry (CV), constant current charge/discharge (CC), electrochemical impedance spectroscopy (EIS) and constant power discharge (CP) methods were used to study the electrochemical performance of EDLCs.

Experimental

Chemicals and reagents used.—1-ethyl-3-methylimidazolium tetrafluoroborate (Sigma-Aldrich, for electrochemistry, $\geq 99.0\%$, H₂O < 200 ppm), zinc chloride ($\geq 97\%$ purity, anhydrous, Sigma-Aldrich) and hydrochloric acid (50% v/v aqueous solution, Alfa Aesar) were used as received. Granulated white sugar (GWS, 17000 kJ/kg, price ~0.45 €/kg) was used for the preparation of sugar solution. 1 M triethylmethylammonium tetrafluoroborate solution in acetonitrile was prepared from pure acetonitrile (H₂O < 0.003%, Riedel-de Haën, stored over molecular sieves before use) and dry triethylmethylammonium tetrafluoroborate (Stella Chemifa Corporation). Ultrapure water

*Electrochemical Society Member.

^zE-mail: alar.janes@ut.ee

(Milli-Q⁺, 18.2 M Ω cm, Millipore) was used for the preparation of the sugar solution, for cleaning the resulting solid product formed during HTC process, and for cleaning the GWS carbon from activating agent and by-products.

Synthesis and physical characterization of GWS carbon material.—The HTC of sugar aqueous solution (17 g of GWS was dissolved in water to prepare 100 ml of solution) was carried out in a high-pressure reactor (Büchi limbo, vessel volume 285 ml) at 200°C for 24 hours. After HTC step, the hydrochar was collected and washed with Milli-Q⁺ water for several times and dried overnight in a vacuum oven (Vaciotem-TV, J.P. Selecta) at 120°C and 50 mbar. The yield of HTC process was 38%.

GWS carbon material was synthesized by activation of the hydrochar with ZnCl₂ with mass ratio 1:4 at 700°C using heating up rate of 5°C min⁻¹. Activation procedure has been carried out according to the method described in Ref. 33 and the yield of this process was 36%. Additional treatment of GWS carbon material with H₂ (purity 99.9999%) at 800°C for 2 hours was performed to reduce the surface functional groups because the H₂ reduced carbon materials demonstrate wider potential region of ideal polarizability.^{27,32,33}

X-ray diffraction (XRD) patterns were collected by a Bruker D8 diffractometer (Bruker Corporation) with position sensitive LynxEye detector using CuK α radiation with an angular step 0.01° and counting time 2 s for each angle measured. Diffraction spectra were recorded at 25°C \pm 1°C temperature. Raman spectra were recorded using a Renishaw inVia micro-Raman spectrometer with Ar laser excitation beam (λ = 514 nm). Obtained spectra were fitted with the combination of two Lorentzian and two Gaussian functions to model the D- and G-bands observed.³⁴

The porous structure of the synthesized GWS carbon material was characterized by the nitrogen sorption method.^{35–37} N₂ sorption experiment was performed at the boiling temperature of liquid nitrogen (–195.8°C) using an ASAP 2020 system (Micromeritics, USA). The specific surface area (S_{BET}) was obtained applying Brunauer-Emmett-Teller (BET)^{36,38} theory to multiple points in the pressure range from 0.05 to 0.1. The total pore volume (V_{tot}) was calculated from the amount of adsorbed nitrogen at relative pressure $p/p_0 = 0.995$. The t -plot method was used to obtain the surface area (S_{micro}) and volume (V_{micro}) of micropores in carbon material studied. The pore size distribution was calculated using a fitting of N₂ isotherm by non-local density functional theory (NLDFT) model “Carbon-N2-77, 2D-NLDFT Heterogeneous Surface” (SAIEUS v2.02, Micromeritics).^{39–43}

The surface structure and morphology of the synthesized hydrochar and carbon material was examined by scanning electron microscopy (SEM), using the ZEISS EVO MA15 SEM system. The surfaces of the samples were sputter-coated with gold before SEM measurements.

Electrode preparation, cell assembly and electrochemical characterization of material.—Carbon electrodes were prepared from synthesized GWS carbon material (94 wt%) adding a 6 wt% suspension of binder (prepared from polytetrafluoroethylene, PTFE, 60% dispersion in H₂O, Sigma-Aldrich). The mixture of synthesized carbon material and binder was laminated and roll-pressed (HS-160N, Hohsen Corporation, Japan) to form a flexible layer of the carbon electrode material with a thickness of 105 \pm 5 μm . After drying under vacuum, for better electrochemical (homogeneous) polarization of carbon layers, the pure Al layer (3 μm) was deposited onto one side of the carbon electrode using the plasma activated physical deposition method. The electrode material loading into one electrode was about 7 mg cm⁻² (mass of binder and current collector are included what were about 10% of the total mass). A standard two-electrode test cell (aluminum, HS Test Cell, Hohsen Corporation) with two identical carbon electrodes (geometric area of 2.0 cm²) and 1 M TEMABF₄ in AN or EMImBF₄ was completed inside a glove box (Labmaster sp, MBraun, O₂ and H₂O concentrations lower than 0.1 ppm). The vacuum dried 25 μm thick TF4425 (Nippon Kodoshi) separator sheet was used to sep-

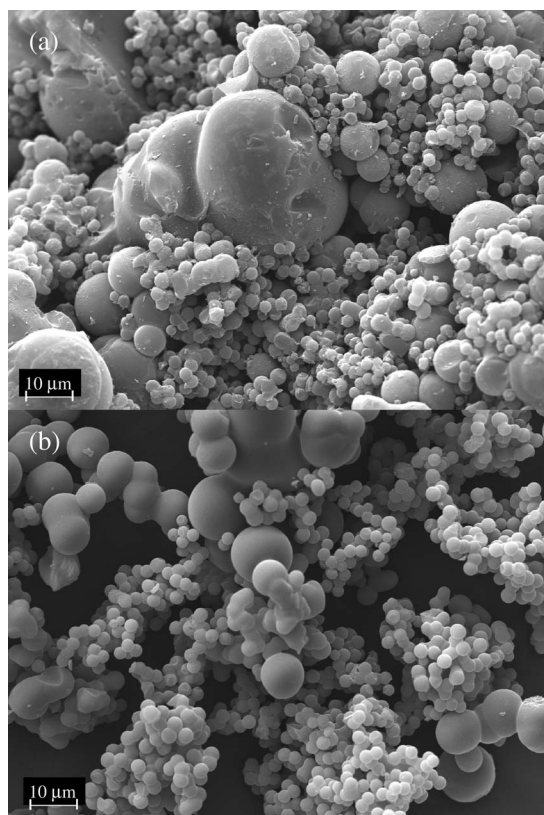


Figure 1. SEM images for hydrochar (a) and GWS carbon material (b).

arate mechanically the two working electrodes. All electrochemical experiments were carried out at temperature 20 \pm 1°C.

The electrochemical characteristics of EDLCs were established by CV, CC, EIS and CP methods. Impedance spectra (over ac frequency range from 1 mHz to 300 kHz with modulation 5 mV), CV and CC curves were recorded using a frequency response analyzer 1252A and potentiostat SI1287 (Solartron, UK). The CP tests were performed on a BT2000 testing system (Arbin Instruments, USA).

Results and Discussion

Physical characterization of GWS carbon material.—The SEM images of the hydrochar and the GWS carbon material are given in Fig. 1. It can be seen that the hydrochar and GWS carbon material exhibit interconnected spheres with various sizes in the range from 1 to 20 μm , which is characteristic of hydrochar and carbon materials synthesized by HTC process.^{15,27,33}

The XRD patterns for synthesized carbon material, given in Fig. 2 inset, show very weak reflections corresponding to the graphite (hexagonal symmetry, space group P6₃/mmc) 002 peak at $2\theta \sim 26^\circ$ and 100/101 peak at $2\theta \sim 43^\circ$, characteristic for mainly amorphous carbon materials.^{6,8,11,16,33}

The first-order Raman spectra, given in Fig. 2, show two characteristic peaks for amorphous carbon materials: one peak at ~ 1338 cm⁻¹ (D-peak) and second peak at ~ 1577 cm⁻¹ (G-peak).^{8,27,28,33,44–47} For hexagonal graphite, G-peak is assigned to E_{2g} vibrational mode, which is attributed to in-plane stretching motion of sp² carbon atom pairs. D-peak originates due to the existence of disorder in a graphitic structure which is assigned to A_{1g} symmetry and this peak reflects the presence of amorphous areas in carbon particles. The ratio of intensities of D-peak and G-peak ($I_{\text{D}}/I_{\text{G}}$) represent the degree of graphitization and a lower value means the higher degree of graphitization.^{33,44–47} Based on D-peak and G-peak fitting results the relatively high value of $I_{\text{D}}/I_{\text{G}}$ (about 1.31) was obtained demonstrating low graphitization degree of

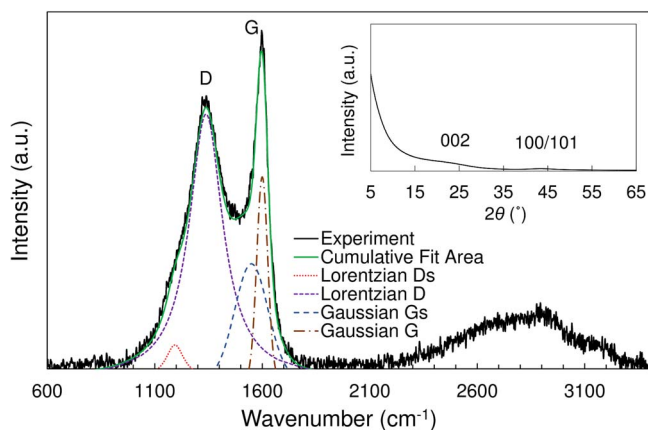


Figure 2. Raman spectra and characteristic XRD patterns (inset) for GWS carbon material.

the GWS carbon, which is in agreement with the XRD results. Thus, Raman spectroscopy and the XRD data reveal that the synthesized carbon material is mainly amorphous.

The N_2 sorption isotherms for the porous GWS carbon material (Fig. 3a) can be approximated to the isotherm of *type I* according to the IUPAC classification,^{37,40} characteristic of microporous carbon material with an average pore width less than 2 nm. According to the porosity measurements results, given in Table I, activation of hydrochar by $ZnCl_2$ produces carbon material with high $S_{BET} = 2100 \text{ m}^2 \text{ g}^{-1}$, $S_{micro} = 2080 \text{ m}^2 \text{ g}^{-1}$, $V_{micro} = 1.01 \text{ cm}^3 \text{ g}^{-1}$ and $V_{tot} = 1.05 \text{ cm}^3 \text{ g}^{-1}$ values. The pore size distribution plot demonstrated in the Fig. 3b shows that

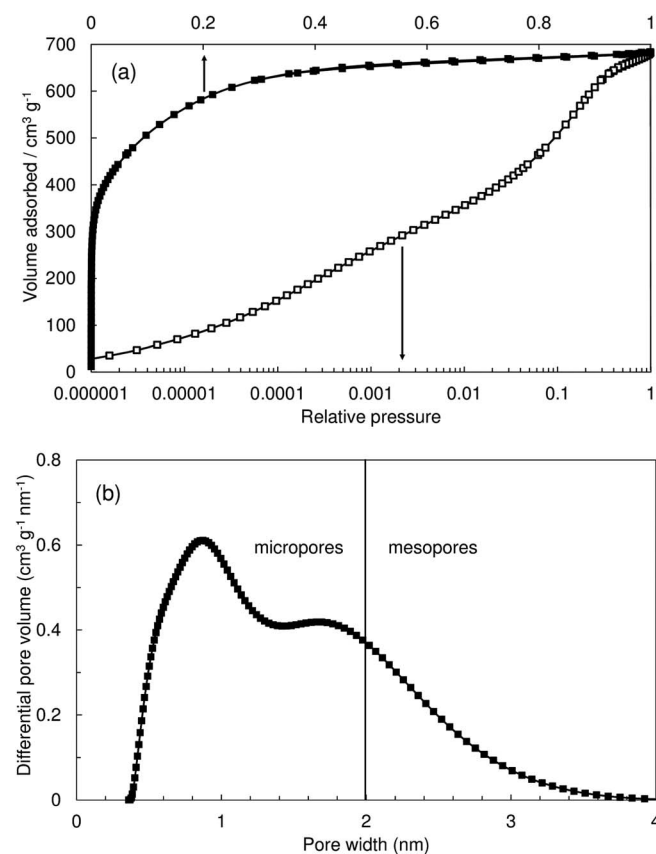


Figure 3. N_2 sorption isotherms (a) and differential pore size distribution vs. pore width plots (b) obtained using NLDFT method in conjunction with SAIEUS pore surface model for GWS carbon material.

Table I. Results of sorption measurements of carbon materials.

Carbon material	S_{BET} ($\text{m}^2 \text{ g}^{-1}$)	S_{micro} ($\text{m}^2 \text{ g}^{-1}$)	V_{micro} ($\text{cm}^3 \text{ g}^{-1}$)	V_{tot} ($\text{cm}^3 \text{ g}^{-1}$)
GWS carbon	2100	2080	1.01	1.05
TiC-CDC-900 ¹¹	1544	1503	0.71	0.87
GDAC-12h ²⁷	1236	1232	0.550	0.557

the GWS carbon material synthesized is highly microporous. However, this carbon material contains also reasonable amount of small mesopores ($2.0 \text{ nm} < d < 3.2 \text{ nm}$). Compared with carbon dioxide activated D-glucose derived carbon,²⁷ $ZnCl_2$, KOH or their mixture activated carbon,³³ different carbide-derived carbons^{8,25,26} and other porous carbon materials,^{5,15,16,19,20} the GWS carbon material demonstrates high specific surface area and micropore surface area as well as total pore volume values, being essential for energy storage materials.

Cyclic voltammetry and capacitance vs. cell potential data.—

The specific capacitance (C_{CV}), calculated from CV curves, vs. cell potential (ΔE) curves for assembled EDLCs are presented in Fig. 4. The C_{CV} values of a test-cell were calculated from CV curves according to Eq. 1 and Eq. 2:

$$C = jv^{-1}, \quad [1]$$

$$C_m = \frac{2C}{m}, \quad [2]$$

where j is the current density (per geometrical surface area of electrode), v is the potential scan rate, C is the cell capacitance and m is the weight of one carbon electrode.

Eq. 1 is correct if the capacitance C does not depend on the potential applied ($C \neq f(\Delta E)$) and the series resistance of the system $R_s \rightarrow 0$, thus, the current response is essentially equal to that of a pure capacitor.^{4,5,11,12,16,20,33} Eq. 2 can be implemented if the positively and negatively charged electrodes have the same capacitance at the cell potential applied.

The specific capacitance vs. cell potential curves for EDLC based on the GWS carbon material in 1 M TEMABF₄ solution in AN and EMImBF₄ ionic liquid have nearly symmetrical shape in respect to the zero-current line at low potential scan rates ($v \leq 50 \text{ mV s}^{-1}$, not shown for clearness of figure) and cell potentials ($\Delta E \leq 3.0 \text{ V}$) demonstrating nearly ideal capacitive behavior (Fig. 4). EDLC based on 1 M TEMABF₄ solution in AN demonstrate nearly ideal capacitive behavior even at very high potential scan rates ($v \leq 500 \text{ mV s}^{-1}$).

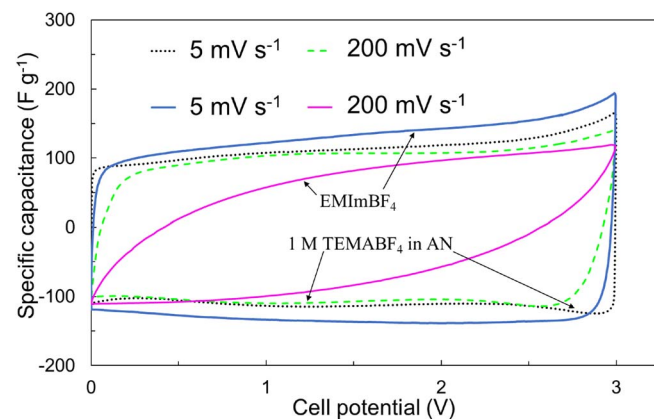


Figure 4. Cyclic voltammetry curves expressed as specific capacitance vs. cell potential dependencies for the EDLCs based on the GWS carbon material in 1 M TEMABF₄ in AN (dotted lines) and EMImBF₄ ionic liquid (solid lines) at cell potential scan rates $v = 5 \text{ mV s}^{-1}$ and $v = 200 \text{ mV s}^{-1}$ (noted in figure) within the cell potential range from 0 to 3.0 V.

Table II. Electrochemical parameters for EDLCs based on different carbon materials and electrolytes.

Carbon material and electrolyte	C_{CV} (F g ⁻¹)	C_{CC} (F g ⁻¹)	C_s (F g ⁻¹)	τ_R (s)
GWS carbon in EMImBF ₄	134	136	144	4.0
GWS carbon in 1 M TEMABF ₄ in AN	110	107	125	0.5
TiC-CDC-900 in 1 M TEMABF ₄ in AN ¹¹	136	N/A	135	0.5
GDAC-12h in 1 M TEMABF ₄ in AN ²⁷	125	N/A	126	0.34

C_{CV} – specific capacitance calculated from CV curves within the cell potential range from 0 to 3.0 V using the integrated charge q obtained according to Eq. 3, C_{CC} – average specific capacitance calculated from CC curves within the cell potential range from 1.5 to 3.0 V, according to Eq. 4, C_s – specific series capacitance calculated from electrochemical impedance data at cell potential $\Delta E = 3.0$ V and ac frequency $f = 1$ mHz, τ_R – characteristic time constant.

However, the highest specific capacitance value $C_{CV} = 134$ F g⁻¹ (at $\Delta E \leq 3.0$ V and $\nu = 1$ mV s⁻¹) has been calculated for EDLC based on the ionic liquid electrolyte (Table II).

The capacitance values have been calculated over the cell potential range ΔE from 0 to 3.0 V, using the integrated total charge q values obtained according to Eq. 3:

$$q = \int_{\Delta E_1}^{\Delta E_2} i(\Delta E) dt \equiv \int_{\Delta E_1}^{\Delta E_2} i(\Delta E) \frac{d(\Delta E)}{\nu} \quad [3]$$

EDLC based on 1 M TEMABF₄ solution in AN demonstrate high capacitance retention and maintain ~70% of the initial capacitance at potential scan rate $\nu = 1000$ mV s⁻¹ showing specific integral capacitance $C_{CV} = 76$ F g⁻¹. Ionic liquid based EDLC system shows somewhat faster capacitance decrease due to the higher viscosity of the ionic liquid. However, this system demonstrated high capacitance retention up to potential scan rate $\nu = 100$ mV s⁻¹ showing specific capacitance $C_{CV} = 94$ F g⁻¹ (~70% of the initial capacitance). At potential scan rate $\nu = 1000$ mV s⁻¹ the specific capacitance decreased to $C_{CV} = 27$ F g⁻¹.

Calculated values of capacitance for GWS carbon material derived from granulated white sugar by HTC and subsequent zinc chloride activation method in 1 M TEMABF₄ solution in AN and EMImBF₄ ionic liquid are comparable with the specific capacitance values established for carbon materials derived from D-glucose^{27,28,33} (i.e. from the more expensive raw material ~40 €/kg). In comparison with binary and ternary carbides (Mo₂C, Ta₄HfC₅, WTiC₂) derived carbons, the GWS carbon offers much cheaper supercapacitor electrodes with comparable or even higher capacitance. In addition, the high-temperature chlorination (or HCl treatment) step can be avoided for the preparation of carbon powders.

Constant current charge/discharge data.—EDLCs were tested at different fixed constant current (CC) regimes (from 0.1 to 5 A g⁻¹) applying charging/discharging steps within cell potential region from 1.5 to 3.0 V. The discharge and charge capacitances have been calculated from the data of the third charge/discharge cycle according to Eq. 4:

$$C = \frac{\int_{\Delta E_1}^{\Delta E_2} j dt}{d(\Delta E)} \quad [4]$$

where j is the current density, dt is the change in time and ΔE is the cell potential. The charge/discharge curves (Figs. 5a and 5b) are nearly linear and symmetrical for EDLCs in 1 M TEMABF₄ solution in AN and EMImBF₄ ionic liquid with carbon electrodes prepared from GWS carbon material at different current densities, demonstrating very good electrochemical reversibility, thus coulombic and energy efficiency. The longest charge/discharge cycle has been observed for EDLC in EMImBF₄ ionic liquid, corresponding to the highest

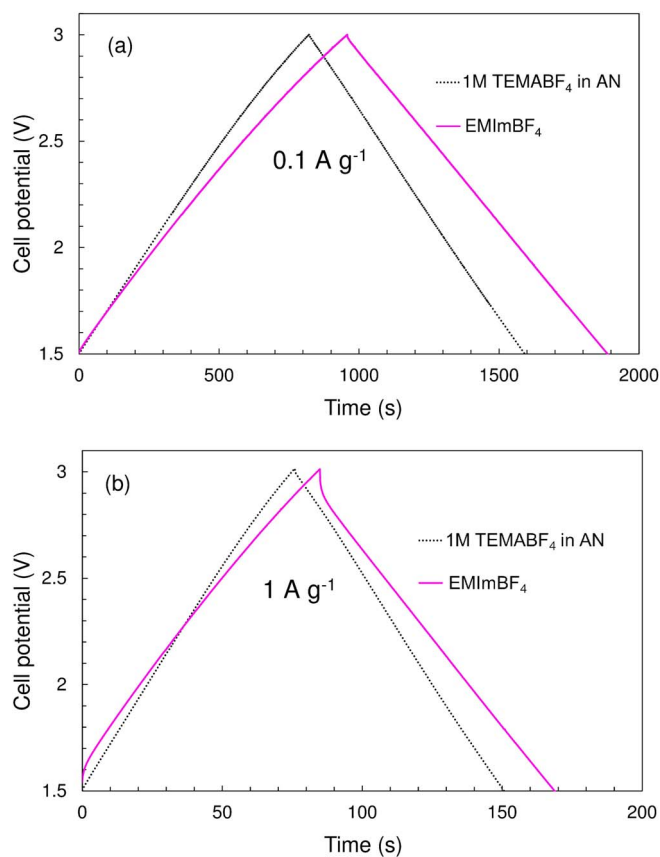


Figure 5. Constant current charge/discharge cycles at current density $j = 0.1$ A g⁻¹ (a) and $j = 1$ A g⁻¹ (b) for the EDLCs based on the GWS carbon material in 1 M TEMABF₄ in AN and EMImBF₄ ionic liquid.

specific capacitance calculated from charge/discharge curves $C_{CC} = 136$ F g⁻¹, being a high value for EDLC in EMImBF₄ ionic liquid electrolyte^{28,32,48-51} (Fig. 5a). EDLC based on 1 M TEMABF₄ solution in AN demonstrated somewhat lower specific capacitance $C_{CC} = 109$ F g⁻¹. The calculated C_{CC} values for EDLCs in both electrolytes are in a good agreement with cyclic voltammetry (Table II) and electrochemical impedance spectroscopy data (discussed later). At higher current densities EDLC based on 1 M TEMABF₄ solution in AN demonstrated high capacitance retention even at current density $j = 5$ A g⁻¹ with the specific capacitance of $C_{CC} = 102$ F g⁻¹. The ionic liquid based EDLC system shows a somewhat faster decrease of capacitance (specific capacitance $C_{CC} = 71$ F g⁻¹ at current density $j = 5$ A g⁻¹) with increased discharge current density.

The cycling efficiency, i.e. the coulombic efficiency (Q_{eff}) values have been calculated as a ratio of integrated charges, measured during discharging and charging steps of EDLCs.⁵² The Q_{eff} values are within the range from 98 to 99%, indicating to a very good reversibility of EDLCs. However, the energy efficiencies (E_{eff}) for studied EDLCs were slightly lower staying within the range from 92 to 97% for TEMABF₄ solution in AN at charging current density range $j = 0.1$ A g⁻¹ to $j = 5$ A g⁻¹, respectively. EMImBF₄ system demonstrated similar (93 to 95%) E_{eff} values for charging current density range $j = 0.1$ A g⁻¹ to $j = 1$ A g⁻¹. However, higher current densities resulted in significantly lower E_{eff} values (77% at $j = 5$ A g⁻¹).

Nyquist plots.—The shape of Nyquist plots (imaginary part $Z(\text{Im})$ vs. real part $Z(\text{Re})$ of the electrochemical impedance) (Fig. 6a)^{1,53,54} depends noticeably on the electrolyte conductivity and viscosity used, but is nearly independent of ΔE applied, if $\Delta E \leq 3.0$ V. This indicates that there are no quick faradaic charge transfer processes at GWS carbon|electrolyte interface. The Nyquist plot (Fig. 6a) con-

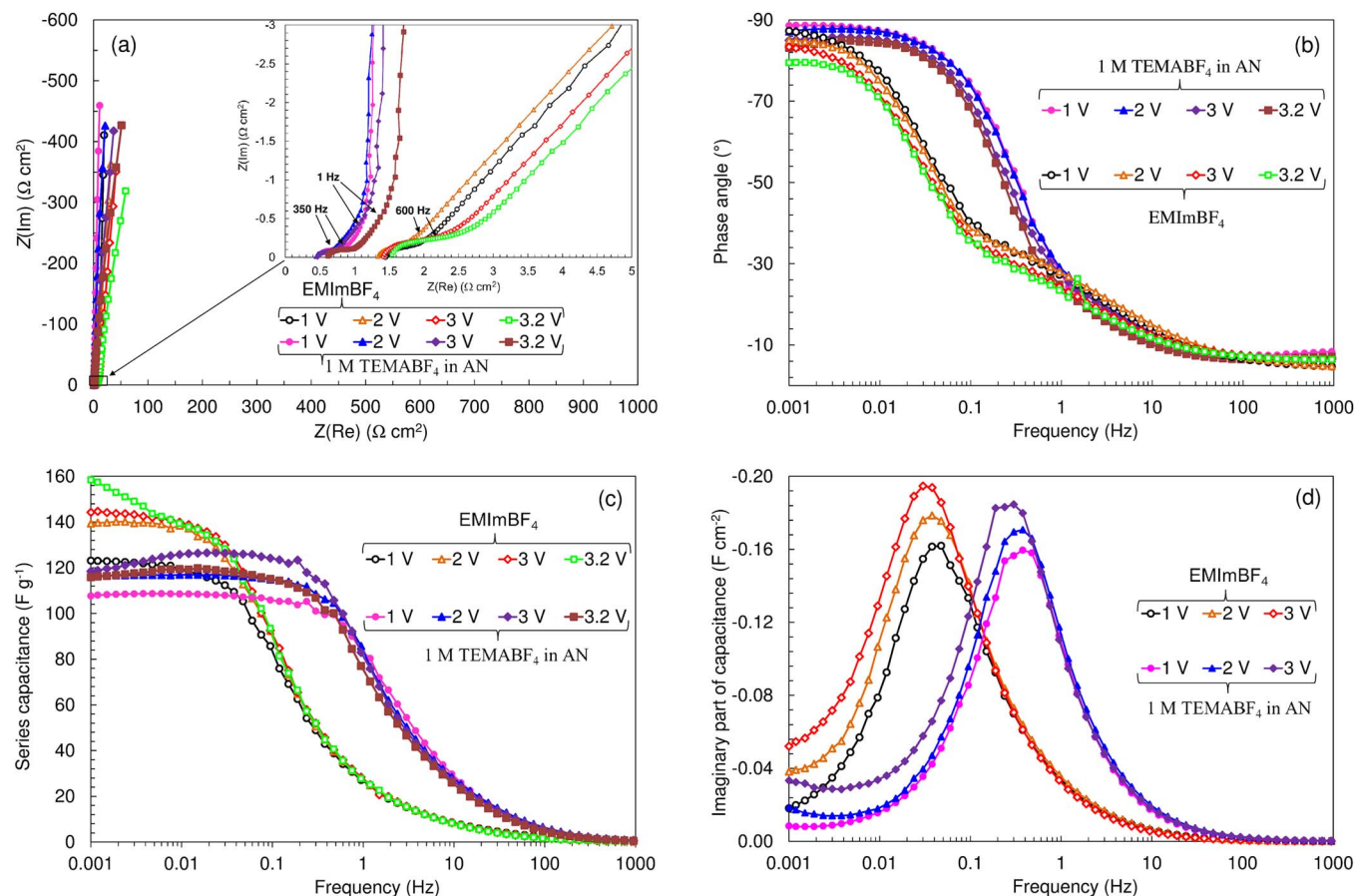


Figure 6. Impedance complex plane plots (a), phase angle vs. ac frequency plots (b), specific series capacitance vs. ac frequency dependencies (c) and imaginary part of capacitance vs. ac frequency plots (d) for the EDLCs based on the GWS carbon material in 1 M TEMABF₄ in AN and EMImBF₄ ionic liquid (noted in figure) at different cell potentials (noted in figure).

sists mainly of three parts: Refs. 11, 28, 33 (1) the characteristic very small semicircle at ac frequencies higher than 300 Hz; (2) the very well expressed so-called “porous” region with a slope of nearly -45° within the ac frequency range from 0.1 to 300 Hz; and (3) the double layer capacitance region with a slope of $\alpha \leq -85^\circ$ at very low ac frequency $f < 0.1$ Hz. The semicircle at high frequencies depends on the adsorption kinetics of ions at the porous carbon electrode and on the series resistance of a material as well as on the mass transfer resistance of electrolyte inside of the porous carbon structure, both being high for ionic liquid based systems. The nearly linear region at intermediate frequencies characterizes the mass transfer limited processes in the porous carbon electrode matrix. The nearly vertical region of the Nyquist plots for the carbons with micro- and mesoporous structure is assigned to the finite length adsorption effects determined by the microporosity of the carbon material under study. Data in Fig. 6a inset show that high frequency series resistance R_s is nearly 3 times higher for EMImBF₄ based EDLC than for TEMABF₄ + AN based EDLC. Therefore, the high-frequency semicircle is more pronounced for EMImBF₄ ionic liquid electrolyte system due to the higher viscosity and lower conductivity of ionic liquid which have a considerable influence on the mass transfer resistance of the electrolyte ions and adsorption capacitance values of porous carbon material.^{11,25,28,33} Data in Fig. 6a inset indicate that the so-called “porous” region with a slope of nearly -45° is well expressed for EDLCs in EMImBF₄, which could be explained by the increased mass-transfer resistance of ions in the porous carbon material for EMImBF₄ ionic liquid electrolyte system.^{11,25,28,32} This observation is in a good accordance with CV and CC data.

The phase angle value for ionic liquid based system (Fig. 6b) approaches -87° and for acetonitrile based electrolyte -89° at low ac

frequencies which demonstrate a nearly ideal capacitive behavior of these systems. The phase angle starts to increase at higher cell potentials $\Delta E \geq 3.0$ V (Fig. 6b) ($|\phi| \leq 80^\circ$ at 3.2 V), especially for ionic liquid based system, due to the initiation of faradaic reactions occurring at highly negatively and positively charged electrodes.^{1,5,14,27,55} The values of specific series capacitance, C_s , (Fig. 6c and Table II), overlapping with C_p values at $f < 0.1$ Hz, and demonstrating long plateaus, are in a good agreement with the values obtained from the CV and CC data. Slightly higher specific capacitance value (140 F g⁻¹) has been achieved for ionic liquid based EDLC system because in CV measurement conditions adsorption equilibrium has not established yet. Only for EMImBF₄ based EDLC noticeable increase of C_s at $\Delta E > 3.2$ V has been observed explained by the very slow faradaic processes.

For further characterization of EDLCs, the values of the imaginary part $C''(\omega)$ of capacitance have been calculated according to the Eq. 5:

$$C''(\omega) = \frac{Z'(\omega)}{\omega|Z(\omega)|^2} \quad [5]$$

where $|Z(\omega)|$ is the impedance modulus.^{53,54} $C''(\omega)$ corresponds to energy dissipation of the capacitor by an irreversible faradaic charge transfer process, which can lead to the hysteresis of the electrochemical processes. According to the results in Fig. 6d, the C'' vs. f dependencies have a well-expressed maximum at the so-called relaxation frequency f_R , determining the characteristic time constant $\tau_R = (2\pi f_R)^{-1}$ values. Comparison of the data for the EDLC systems completed with different electrolytes indicates a very strong influence of electrolyte properties on τ_R values (Table II). The value of τ_R in-

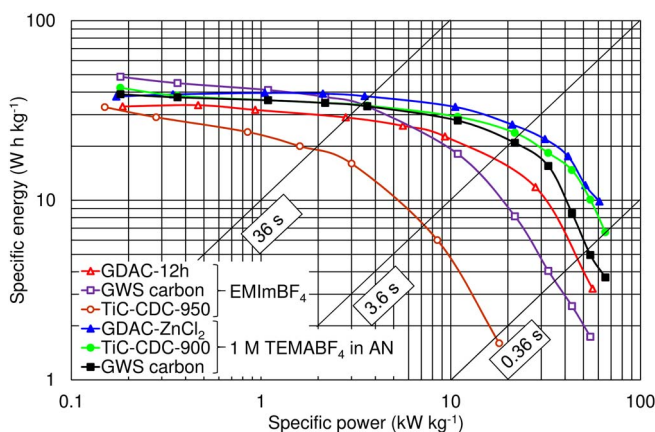


Figure 7. Specific energy vs. specific power plots for the EDLCs based on different carbon materials in 1 M TEMABF₄ in AN and EMImBF₄ ionic liquid (noted in figure), obtained from constant power tests within the cell potential range from 3.0 V to 1.5 V.

creases with the decrease of electrolyte conductivity and increase of electrolyte viscosity, but the value of τ_R is only slightly dependent of ΔE applied, at $\Delta E \leq 3.0$ V. The characteristic time constant values for EDLCs in 1 M TEMABF₄ solution in AN and EMImBF₄ ionic liquid are $\tau_R \sim 0.5$ s and $\tau_R \sim 4.0$ s, respectively.

The τ_R value established for EDLCs in 1 M TEMABF₄ solution in AN ($\tau_R \sim 0.5$ s) is substantially shorter than that of the carbon material synthesized from natural organic precursor (cellulose, potato starch, eucalyptus wood sawdust) using HTC process followed by the subsequent KOH activation ($\tau_R \sim 10$ s).²⁰ The calculated τ_R values are comparable with τ_R for EDLCs based on D-glucose derived carbon electrodes (carbon material activated for 12 h with carbon dioxide ($\tau_R = 0.34$ s)),²⁷ for activated sucrose-derived carbon electrodes ($\tau_R \sim 0.5$ s)⁴⁸ and for KOH and ZnCl₂ activated carbon electrodes ($\tau_R \sim 0.8$ s)³³ based EDLCs.

The τ_R value obtained for EDLC based on the GWS carbon material in EMImBF₄ ionic liquid ($\tau_R = 4.2$ s) is substantially shorter than τ_R obtained for sucrose derived carbon ($\tau_R = 20$ s),⁵⁶ coconut shell activated carbon ($\tau_R \sim 10$ s)⁵¹ and for carbon cloth ($\tau_R = 8$ s)²⁹ and only slightly longer compared with characteristic time constant obtained for carbon nanosheets ($\tau_R \sim 2.5$ s)⁵⁷ and titanium carbide-derived carbon based EDLC ($\tau_R = 1.76$ s).⁵⁸

Ragone plots.—The Ragone plots, i.e. the energy vs. power relationships^{1,2,27,32,59} for the EDLCs in 1 M TEMABF₄ solution in AN and EMImBF₄ ionic liquid have been calculated from the constant power discharge tests within the cell potential range from 3.0 V to 1.5 V (Fig. 7) (taking into account the total weight of electrodes, i.e. mass of carbon material, binder and current collectors). The specific energy vs. specific power plots for the EDLCs based on GWS carbon material and 1 M TEMABF₄ solution in AN or EMImBF₄ ionic liquid show a noticeable influence of the electrolyte properties, i.e. viscosity and electrical conductivity on the stored specific energy and delivered specific power values. At low constant power values, the stored energy is somewhat higher for EDLC based EMImBF₄ ionic liquid (48 W h kg⁻¹) in a good agreement with the specific capacitance values obtained from the CV, CC and EIS data. At higher constant power values the EDLC based on 1 M TEMABF₄ solution in AN electrolyte deliver substantially higher energy due to the lower viscosity and higher electrical conductivity compared to the ionic liquid based EDLC.

For comparison of the achieved energy- and power density values established in this work, similar dependencies for the titanium carbide-derived carbon material synthesized at chlorination temperature 900°C (TiC-CDC-900)¹¹ and for D-glucose derived zinc chloride activated carbon material (GDAC-ZnCl₂)³³ based systems in 1 M TEMABF₄ solution in AN, the titanium carbide-derived carbon mate-

rial synthesized at chlorination temperature 950°C (TiC-CDC-950)⁶⁰ and for carbon dioxide activated D-glucose derived carbon material (GDAC-12h)²⁸ based systems in EMImBF₄ ionic liquid have been introduced into Fig. 7. These results show that GWS carbon material synthesized in this work exhibit similar energy density values at low constant power values (39 W h kg⁻¹) and slightly lower energy density values at higher constant power values in 1 M TEMABF₄ solution in AN compared with TiC-CDC-900 and GDAC-ZnCl₂ carbons based EDLCs. However, in EMImBF₄ ionic liquid electrolyte GWS carbon material shows the highest energy density at low constant power values (48 W h kg⁻¹) compared with GDAC-12h and TiC-CDC-950 carbon materials and slightly lower energy density values at higher constant power values compared with GDAC-12h carbon based EDLC.

Conclusions

Granulated white sugar derived carbon (GWS carbon) material was synthesized from hydrochar, obtained from hydrothermal carbonization of granulated white sugar (GWS) aqueous solution, applying additional activation with ZnCl₂ in mass ratio 1:4 at the temperature 700°C.

Based on the XRD and Raman spectroscopy data, the synthesized GWS carbon material is mainly amorphous. N₂ sorption measurements results show that GWS carbon material is mainly microporous, however, this carbon contains also reasonable amount of small mesopores and shows high porosity, i.e. high Brunauer-Emmett-Teller specific surface area $S_{BET} = 2100$ m² g⁻¹, micropore surface area $S_{micro} = 2080$ m² g⁻¹, micropore pore volume $V_{micro} = 1.01$ cm³ g⁻¹ and total pore volume $V_{tot} = 1.05$ cm³ g⁻¹.

The electrochemical characteristics of the EDLCs consisting of the GWS carbon material based electrodes in 1 M triethylmethylammonium tetrafluoroborate (TEMABF₄) solution in acetonitrile (AN) and in 1-ethyl-3-methylimidazolium tetrafluoroborate ionic liquid (EMImBF₄) were tested applying the electrochemical impedance spectroscopy, cyclic voltammetry, constant current charge/discharge and the constant power discharge methods.

The electrochemical impedance spectroscopy, cyclic voltammetry and constant current charge/discharge measurement results show that the values of specific capacitance are somewhat higher for EMImBF₄ (135 ± 5 F g⁻¹) electrolyte compared to the TEMABF₄ in AN (110 ± 5 F g⁻¹). The specific energy vs. specific power dependencies are similar with the previous results and at low constant power values the stored energy is higher for EDLC based on EMImBF₄ ionic liquid (48 W h kg⁻¹) compared with EDLC based on TEMABF₄ in AN electrolyte (39 W h kg⁻¹). However, the best capacitance retention and shortest relaxation time constant $\tau_R \sim 0.5$ s were established for EDLCs in 1 M TEMABF₄ solution in AN due to the lower viscosity and higher electrical conductivity compared to the ionic liquid based electrolyte. Therefore, EDLC based on 1 M TEMABF₄ solution in AN electrolyte delivers substantially higher energy at higher constant power values.

Thus, the GWS carbon material synthesized using cheap and abundant GWS as the starting material, show good electrochemical performance in TEMABF₄ in AN as well in EMImBF₄ ionic liquid and is promising carbon material for the high energy and power density supercapacitor application. It is important to mention that synthesis of carbon nanospheres is simpler and environmentally more friendly than the preparation of molybdenum carbide or titanium carbide derived carbon powders. As a next step, the carbon powders will be synthesized from the raw syrup or from the molasses of different plants (thus less expensive than GWS) and tested as electrode materials for EDLC and other devices.

Acknowledgments

This research was supported by the EU through the European Regional Development Fund (Centers of Excellence, 2014–2020.4.01.15-0011 and 3.2.0101-0030, TeRa project SLOKT12026T. Higher education specialization stipends in smart specialization

growth areas 2014–2020.4.02.16-0026) and Institutional Research grant IUT20–13. This work was partially supported by Estonian Research Council grants PUT1033 and PUT55.

References

- B. E. Conway, *Electrochemical supercapacitors: scientific fundamentals and technological applications*, Springer, New York (1999).
- R. Kötz and M. Carlen, *Electrochim. Acta*, **45**, 2483 (2000).
- A. Burke, *J. Power Sources*, **91**, 37 (2000).
- G. Salitra, A. Soffer, L. Eliad, Y. Cohen, and D. Aurbach, *J. Electrochem. Soc.*, **147**, 2486 (2000).
- E. Frackowiak and F. Beguin, *Carbon*, **39**, 937 (2001).
- T. Thomborg, H. Kurig, A. Jänes, and E. Lust, *Micropor. Mesopor. Mater.*, **141**, 88 (2011).
- A. Burke and M. Miller, *J. Power Sources*, **196**, 514 (2011).
- I. Tallo, T. Thomborg, K. Kontturi, A. Jänes, and E. Lust, *Carbon*, **49**, 4427 (2011).
- L. Eliad, G. Salitra, A. Soffer, and D. Aurbach, *Langmuir*, **21**, 3198 (2005).
- Gogotsi, A. Nikitin, H. Ye, W. Zhou, J. E. Fischer, B. Yi, H. C. Foley, and M. W. Barsoum, *Nat. Mater.*, **2**, 591 (2003).
- I. Tallo, T. Thomborg, H. Kurig, A. Jänes, K. Kontturi, and E. Lust, *J. Solid State Electrochem.*, **17**, 19 (2013).
- J. Chmiola, G. Yushin, R. Dash, and Y. Gogotsi, *J. Power Sources*, **158**, 765 (2006).
- M. Oschatz, E. Kockrick, M. Rose, L. Borchardt, N. Klein, I. Senkovska, T. Freudenberg, Y. Korenblit, G. Yushin, and S. Kaskel, *Carbon*, **48**, 3987 (2010).
- I. Tallo, T. Thomborg, A. Jänes, and E. Lust, *J. Electrochem. Soc.*, **159**, A208 (2012).
- M.-M. Titirici, Ed., *Sustainable carbon materials from hydrothermal processes*, p. 357, Wiley, Chichester (2013).
- Q.-Y. Li, H.-Q. Wang, Q.-F. Dai, J.-H. Yang, and Y.-L. Zhong, *Solid State Ion*, **179**, 269 (2008).
- R. Demir-Cakan, N. Baccile, M. Antonietti, and M.-M. Titirici, *Chem. Mater.*, **21**, 484 (2009).
- W. Zhang, H. Tao, B. Zhang, J. Ren, G. Lu, and Y. Wang, *Carbon*, **49**, 1811 (2011).
- H. Zhu, X. Wang, F. Yang, and X. Yang, *Adv. Mater.*, **23**, 2745 (2011).
- L. Wei, M. Sevilla, A. B. Fuertes, R. Mokaya, and G. Yushin, *Adv. Energy Mater.*, **1**, 356 (2011).
- K. Kinoshita, *Carbon: Electrochemical and Physicochemical Properties*, 1 edition., p. 560, Wiley, New York (1988).
- H. Marsh and F. R. Reinoso, *Activated Carbon*, p. 555, Elsevier, London (2006).
- M. Arulepp, L. Permann, J. Leis, A. Perkson, K. Rumma, A. Jänes, and E. Lust, *J. Power Sources*, **133**, 320 (2004).
- A. Jänes and E. Lust, *J. Electroanal. Chem.*, **588**, 285 (2006).
- E. Tee, I. Tallo, H. Kurig, T. Thomborg, A. Jänes, and E. Lust, *Electrochim. Acta*, **161**, 364 (2015).
- I. Tallo, T. Thomborg, H. Kurig, K. Kontturi, A. Jänes, and E. Lust, *Carbon*, **67**, 607 (2014).
- T. Thomborg, T. Tooming, T. Romann, R. Palm, A. Jänes, and E. Lust, *J. Electrochem. Soc.*, **160**, A1834 (2013).
- T. Tooming, T. Thomborg, H. Kurig, A. Jänes, and E. Lust, *J. Power Sources*, **280**, 667 (2015).
- H. Kurig, M. Vestli, K. Tönurist, A. Jänes, and E. Lust, *J. Electrochem. Soc.*, **159**, A944 (2012).
- S. Zhang, N. Sun, X. He, X. Lu, and X. Zhang, *J. Phys. Chem. Ref. Data*, **35**, 1475 (2006).
- M. Galiński, A. Lewandowski, and I. Stepniak, *Electrochim. Acta*, **51**, 5567 (2006).
- T. Tooming, T. Thomborg, L. Siinor, K. Tönurist, A. Jänes, and E. Lust, *J. Electrochem. Soc.*, **161**, A222 (2014).
- M. Härmas, T. Thomborg, H. Kurig, T. Romann, A. Jänes, and E. Lust, *J. Power Sources*, **326**, 624 (2016).
- J. Ribeiro-Soares, M. E. Oliveros, C. Garin, M. V. David, L. G. P. Martins, C. A. Almeida, E. H. Martins-Ferreira, K. Takai, T. Enoki, R. Magalhães-Paniago, A. Malachias, A. Jorio, B. S. Archanjo, C. A. Achete, and L. G. Cançado, *Carbon*, **95**, 646 (2015).
- P. I. Ravikovitch and A. V. Neimark, *Colloids Surf. Physicochem. Eng. Asp.*, **187–188**, 11 (2001).
- S. Brunauer, P. H. Emmett, and E. Teller, *J. Am. Chem. Soc.*, **60**, 309 (1938).
- S. J. Gregg and K. S. W. Sing, *Adsorption, surface area, and porosity*, p. 328, Academic Press, (1991).
- S. Brunauer, L. S. Deming, W. E. Deming, and E. Teller, *J. Am. Chem. Soc.*, **62**, 1723 (1940).
- P. I. Ravikovitch, A. Vishnyakov, and A. V. Neimark, *Phys. Rev. E*, **64**, 0116021 (2001).
- J. Rouquerol, F. Rouquerol, and K. S. W. Sing, *Adsorption by Powders and Porous Solids: Principles, Methodology and Applications*, 1 edition., p. 467, Academic Press, San Diego (1998).
- W. D. Harkins and G. Jura, *J. Am. Chem. Soc.*, **66**, 1366 (1944).
- J. Jagiello, *Langmuir*, **10**, 2778 (1994).
- J. Jagiello and J. P. Olivier, *Adsorption*, **19**, 777 (2013).
- F. Tuinstra and J. L. Koenig, *J. Chem. Phys.*, **53**, 1126 (1970).
- A. C. Ferrari, *Solid State Commun.*, **143**, 47 (2007).
- M. S. Dresselhaus, G. Dresselhaus, and M. Hofmann, *Vib. Spectrosc.*, **45**, 71 (2007).
- H. Kurig, M. Russina, I. Tallo, M. Siebenbürger, T. Romann, and E. Lust, *Carbon*, **100**, 617 (2016).
- L. Wei and G. Yushin, *Carbon*, **49**, 4830 (2011).
- A. Lewandowski and M. Galiński, *J. Phys. Chem. Solids*, **65**, 281 (2004).
- G. Sun, K. Li, L. Xie, J. Wang, and Y. Li, *Micropor. Mesopor. Mater.*, **151**, 282 (2012).
- M. Galinski, K. Babel, and K. Jurewicz, *J. Power Sources*, **228**, 83 (2013).
- A. Laheäär, P. Przygocki, Q. Abbas, and F. Béguin, *Electrochem. Commun.*, **60**, 21 (2015).
- E. Barsouk and J. R. Macdonald, *Impedance spectroscopy: theory, experiment, and applications*, Wiley, John & Sons, Inc., (2005).
- P. L. Taberna, P. Simon, and J. F. Fauvarque, *J. Electrochem. Soc.*, **150**, A292 (2003).
- T. Romann, O. Oll, P. Pikma, H. Tamme, and E. Lust, *Electrochim. Acta*, **125**, 183 (2014).
- L. Wei and G. Yushin, *J. Power Sources*, **196**, 4072 (2011).
- D. Zhou, H. Wang, N. Mao, Y. Chen, Y. Zhou, T. Yin, H. Xie, W. Liu, S. Chen, and X. Wang, *Micropor. Mesopor. Mater.*, **241**, 202 (2017).
- H. Kurig, A. Jänes, and E. Lust, *J. Electrochem. Soc.*, **157**, A272 (2010).
- K. Tönurist, T. Thomborg, A. Jänes, and E. Lust, *J. Electrochem. Soc.*, **160**, A449 (2013).
- K. Tönurist, T. Thomborg, A. Jänes, I. Kink, and E. Lust, *Electrochem. Commun.*, **22**, 77 (2012).